Modelling Soil Erosion, Sediment Transport and Closely Related Hydrological Processes (Proceedings of a symposium held at Vienna, July 1998). IAHS Publ. no. 249, 1998.

Multi-scale Green's function Monte Carlo approach to erosion modelling and its application to land-use optimization

LUBOS MITAS
National Center for Supercomputing Applications, 405 N. Mathews Avenue, University of Illinois at Urbana-Champaign, Urbana, Illinois 61801, USA

HELENA MITASOVA
Geographic Modeling Systems Laboratory, Department of Geography, 220 Davenport Hall, University of Illinois at Urbana-Champaign, Urbana, Illinois, USA

Abstract A new generation of simulation tools for modelling soil erosion, sediment transport and deposition by overland water flow in complex landscapes is presented. The simulations are based on the solution of bivariate continuity equations describing water and sediment transport over 3D terrain with variable climatic, soil and land-cover conditions. The underlying equations are solved by advanced computational approaches based on stochastic projection techniques (Green's function Monte Carlo), providing the robustness and flexibility necessary for complex conditions and multi-scale implementation with spatially variable accuracy/resolution. The processing, analysis and visualization of data and results are performed using an emerging multidimensional dynamic GIS technology. The possibilities of using the simulations as a tool for finding optimal land-use patterns with minimized erosion risk are evaluated by comparing computer optimized land-use scenario with the traditional land-use design.

INTRODUCTION

Effectiveness of land management decisions aimed towards preventing negative impacts of soil erosion in complex landscapes can be significantly improved by detailed predictions of erosion and deposition patterns for proposed land-use alternatives. Advances in GIS technology stimulate the replacement of traditional lumped empirical models by process-based distributed ones (Moore *et al.*, 1993; Maidment, 1996; Saghafian *et al.*, 1995; Suri & Hofierka, 1994) which have a potential to provide the needed predictions. In spite of a significant progress in this area of research, applications of distributed models are still rather laborious and often results do not have sufficient detail, accuracy and realism for basin-scale land management purposes. In this paper, we try to address some of these problems by focusing on:

(a) description of processes by "first principles" relations in a bivariate form allowing us to incorporate a full impact of complex terrain, soil and cover conditions;
(b) use of robust solvers (Green's function Monte Carlo) which minimize the manual preprocessing of data and work efficiently on parallel architectures;
(c) investigations of computer simulated scenarios for finding optimal land-use patterns with minimized erosion risk;
(d) investigation of multi-scale implementations of the above-mentioned robust solvers for studies of areas with variable accuracy and resolution;

(e) increase efficiency by extensive use of GIS for processing, analysis and visualization of the data and results, as described in detail by Mitasova *et al.* (1995); Mitas *et al.* (1997).

METHODS

Water and sediment transport

The model used in this paper is described by Mitas & Mitasova (1998), therefore here we briefly present only its principles. A bivariate shallow water flow continuity equation for a rainfall event (e.g. Saghafian *et al.*, 1995) is given by:

$$\frac{\partial h(\mathbf{r},t)}{\partial t} = i_e(\mathbf{r},t) - \nabla\cdot[h(\mathbf{r},t)\mathbf{v}(\mathbf{r},t)] \tag{1}$$

where $h(\mathbf{r},t)$ [m] is the depth of overland flow, $i_e(\mathbf{r},t)$ [m s^{-1}] is the rainfall excess, $\mathbf{v}(\mathbf{r},t)$ [m s^{-1}] is velocity and $\mathbf{r} = (x,y)$ [m] is the position. The equation (1) is coupled with the momentum conservation equation (in the diffusive wave approximation) which together with the Manning's relation between the depth and velocity create a closed system of equations. The steady-state form of equation (1) is given by:

$$-\frac{\varepsilon}{2}\nabla^2[h^{5/3}(\mathbf{r})] + \nabla\cdot\mathbf{q}(\mathbf{r}) = i_e(\mathbf{r}) \tag{2}$$

where $\mathbf{q}(\mathbf{r})$ [m^2 s^{-1}] is the water flow per unit width and the diffusive wave effects are incorporated approximately by the term $\propto\nabla^2[h^{5/3}(\mathbf{r})]$.

Overland water flow is the driving force for hillslope erosion which includes sediment entrainment, transport and deposition. The continuity of sediment mass is given by:

$$\frac{\partial[\rho_s c(\mathbf{r},t)h(\mathbf{r},t)]}{\partial t} - \frac{\omega}{2}\nabla^2[\rho_s c(\mathbf{r},t)h(\mathbf{r},t)] + \nabla\cdot\mathbf{q}_s(\mathbf{r},t) = \text{sources} - \text{sinks} = D(\mathbf{r},t) \tag{3}$$

where $\mathbf{q}_s(\mathbf{r},t) = \rho_s c(\mathbf{r},t)\mathbf{q}(\mathbf{r},t)$ [kg m^{-1} s^{-1}] is the sediment flow rate per unit width, $c(\mathbf{r},t)$ [particle m^{-3}] is sediment concentration, ρ_s [kg particle^{-1}] is mass per sediment particle, and ω [m^2 s^{-1}] characterizes local dissipation (diffusion) processes. For a steady-state case the equation is:

$$-\frac{\omega}{2}\nabla^2[\rho_s c(\mathbf{r})h(\mathbf{r})] + \nabla\cdot\mathbf{q}_s(\mathbf{r}) = D(\mathbf{r}) \tag{4}$$

The source/sink term $D(\mathbf{r})$ in equation (4) is similar to the one used by Foster & Meyer (1972), namely $D(\mathbf{r}) = \sigma(\mathbf{r})[T(\mathbf{r}) - |\mathbf{q}_s(\mathbf{r})|]$, where $T(\mathbf{r})$ [kg m^{-1} s^{-1})] is the sediment transport capacity, $\sigma(\mathbf{r}) = D_c(\mathbf{r})/T(\mathbf{r})$ [m^{-1}] is the first-order reaction term and D_c (**r**) [kg m^{-2} s^{-1}] is the detachment capacity. Both $T(\mathbf{r})$ and D_c (**r**) are functions of shear stress (Flanagan & Nearing, 1995). In addition, we also tested a new form of $T(\mathbf{r})$ which depends on stream power, as suggested very recently by Nearing *et al.* (1997).

Multi-scale/spatially variable Green's function Monte Carlo method

In this section we outline the solution of the above presented transport by stochastic techniques with variable resolution. Because of space constraints, we consider only the steady-state cases given by equations (2) and (4), however, methodology is similar also for the time-dependent cases. The equations (2), (4) have a general form in which a linear differential operator $\mathcal{O}$ acts on a nonnegative function $\gamma(\mathbf{r})$ (either $h(\mathbf{r})$ or $\rho_s c(\mathbf{r})h(\mathbf{r})$), while on the right-hand side, there is a source term $\mathcal{S}(\mathbf{r})$:

$$\mathcal{O}\gamma(\mathbf{r}) = \mathcal{S}(\mathbf{r}) \tag{5}$$

Using the Green's function $G(\mathbf{r},\mathbf{r}',p)$ the solution can be expressed as:

$$\gamma(\mathbf{r}) = \int_0^\infty \int G(\mathbf{r},\mathbf{r}',p)\,\mathcal{S}(\mathbf{r}')\,\mathrm{d}\mathbf{r}'\mathrm{d}p \tag{6}$$

while $G(\mathbf{r},\mathbf{r}',p)$ is given by the following equation and an initial condition:

$$\frac{\partial G(\mathbf{r},\mathbf{r}',p)}{\partial p} = -\mathcal{O}\,G(\mathbf{r},\mathbf{r}',p);\; G(\mathbf{r},\mathbf{r}',0) = \delta(\mathbf{r}-\mathbf{r}') \tag{7}$$

where δ is the Dirac function. In addition, we assume that the spatial region is a delineated drainage basin with zero boundary condition which is fulfilled by $G(\mathbf{r},\mathbf{r}',p)$.

Equations (1–4) can be interpreted as Fokker-Planck stochastic processes (Gardiner, 1985) with diffusion and drift components. Such an interpretation opens new possibilities to solve these equations through a *simulation* of the underlying process utilizing stochastic methods (Gardiner, 1985). This type of Monte Carlo approach is one of the modern alternatives to finite element or finite difference approaches and is being explored in computational fluid dynamics or in quantum Monte Carlo methods for solving the Schrödinger equation (see Mitas, 1996; and references therein). Very briefly, the solution is obtained as follows. A number of sampling points distributed according to the source $\mathcal{S}(\mathbf{r}')$ is generated. The sampling points are then propagated according to the function $G(\mathbf{r},\mathbf{r}',p)$ and averaging of path samples provides an estimation of the actual solution $\gamma(\mathbf{r})$ with a statistical accuracy proportional to $1/\sqrt{M}$ where M is the number of samples. An animated illustration of this method can be found in Mitas *et al.* (1997). The Monte Carlo technique has several unique advantages when compared with more traditional methods. It is very robust and enables studies for spatially complex cases with the minimum manual preprocessing of input data. Moreover, rough solutions, which identify the major sediment concentrations and erosion/deposition patterns can be estimated quickly, allowing us to carry out preliminary quantitative studies or to rapidly extract qualitative trends by parameter scans. In addition, Monte Carlo methods are tailored to the new generation of computers as they provide scalability from a single workstation to large parallel machines due to the independence of sampling points. Therefore, the methods are useful both for everyday exploratory work using a desktop computer and for large, cutting-edge applications using high performance computing.

Furthermore, solution through the Green's function given by equation (6) can be elegantly reformulated for accommodation of *spatially variable accuracy* and *resolution*. The integral (6) can be multiplied by a *reweighting* function $W(\mathbf{r})$:

$$W(\mathbf{r})\gamma(\mathbf{r}) = \int_0^\infty \int W(\mathbf{r})G(\mathbf{r},\mathbf{r}',p)\,\mathcal{S}(\mathbf{r}')\,\mathrm{d}\mathbf{r}'\mathrm{d}p = \int_0^\infty \int G^*(\mathbf{r},\mathbf{r}',p)\,\mathcal{S}(\mathbf{r}')\,\mathrm{d}\mathbf{r}'\mathrm{d}p \qquad (8)$$

which is equal to the appropriate increase in accuracy ($W(\mathbf{r}) > 1$) in the regions of

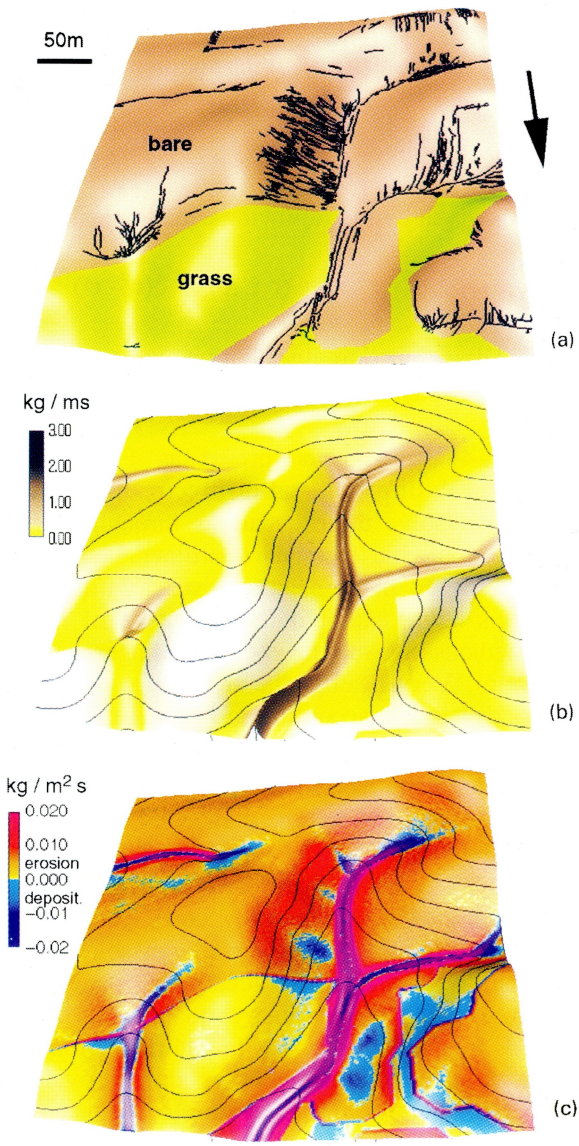

Fig. 1 Terrain model with (a) traditional land use and linear erosion features, (b) simulated sediment flow, (c) erosion/deposition pattern for bare soil in the agricultural field and a 70 mm h^{-1} rainfall excess.

interest while it is unity elsewhere. The function $W(\mathbf{r})$ can change (abruptly or smoothly) between regions with unequal resolutions and in fact, can be optimally adapted to the quality of input data (terrain, soils, etc.) so that the accurate solution is calculated only in the regions with correspondingly accurate inputs. The reweighted Green's function $G^*(\mathbf{r},\mathbf{r}',p)$, in effect, introduces higher density of sampling points in the region with large $W(\mathbf{r})$. The statistical noise will be spatially variable as $\approx 1/[W(\mathbf{r})\sqrt{M}]$, where M is the average number of samples resulting in the

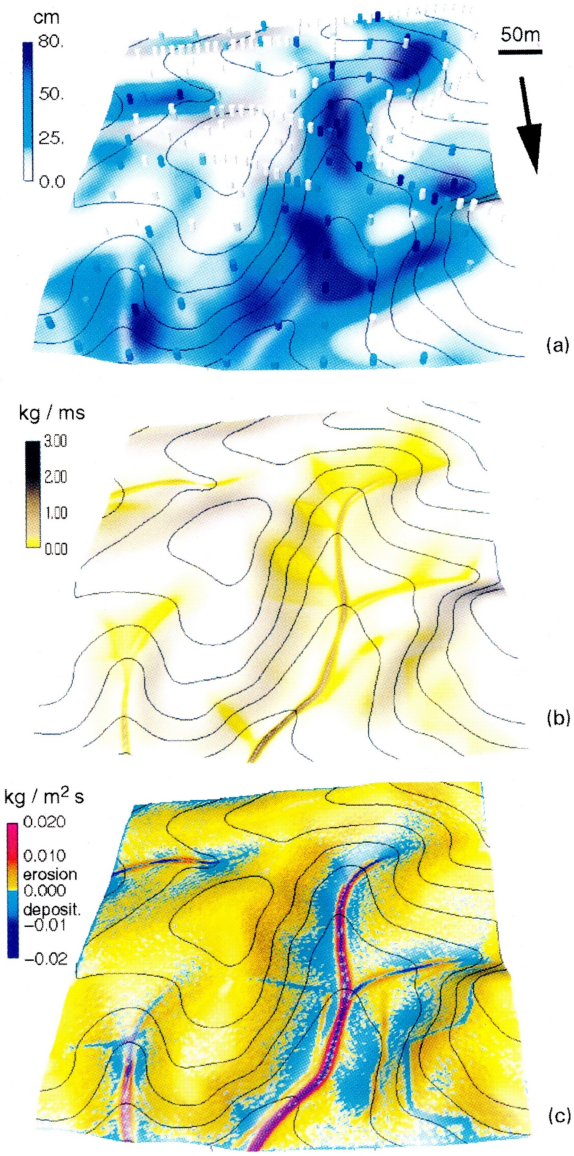

Fig. 2 Terrain model with (a) observed depths of colluvial deposits, (b) simulated sediment flow, (c) erosion/deposition pattern for vegetative cover in the agricultural field and a 20 mm h^{-1} rainfall excess.

accuracy increase for the areas with $W(\mathbf{r}) > 1$.

Large areas are often characterized by data with variable resolution and the above *multi-scale* formulation is able to make the best use of such heterogeneous data. Another reason why one would like to change the resolution and accuracy is the desire of the user: very often the area of interest is rather small, however, it requires inputs from a much larger region. The system of equations (1)–(4) describes the water and sediment flow at a spatial scale equal or larger than an average distance

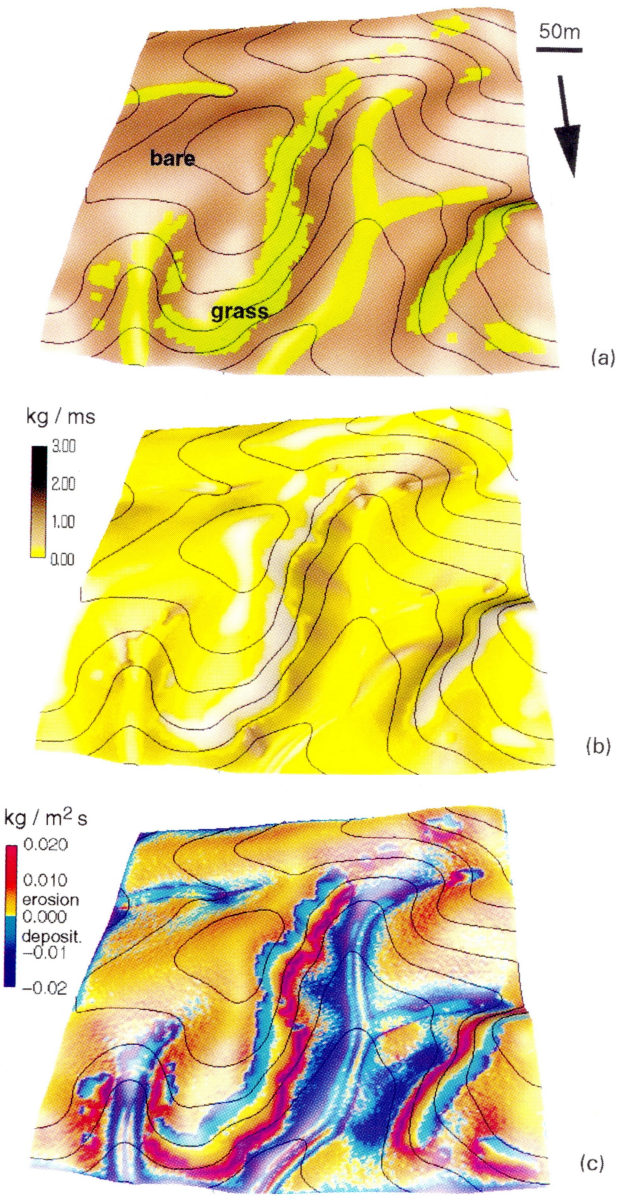

Fig. 3 Terrain model with (a) computer designed land use, (b) simulated sediment flow, (c) erosion/deposition pattern for bare soil in the agricultural field and a 70 mm h^{-1} rainfall excess.

between rills (i.e. grid cell size ≥ 1 m) and therefore the presented approach allows us to perform landscape scale simulations at variable spatial resolutions from one to hundreds of metres, depending on the complexity and importance of the subregions studied.

The presented model was implemented as an independent computational module named SIMWE (SIMulation of Water Erosion) and linked to the GRASS GIS.

RESULTS

High resolution erosion and deposition patterns in spatially complex conditions

We have evaluated the capabilities of the presented model using an ≈ 1 km^2 subarea of the Scheyern experimental farm (Auerswald *et al.*, 1996). The measured elevation data were interpolated to a 2 m resolution DEM by regularized spline with tension (Mitasova & Mitas, 1993) and land cover and soil data were used to estimate erodibility and transportability parameters based on the literature (Foster & Meyer, 1972; Flanagan & Nearing, 1995).

First, we have applied the model for traditional land-use (Fig. 1(a)—please note that colour versions of figures are available at: http://www2.gis.uiuc.edu:2280/modviz/papers/iahsav30.html) for two different situations: (a) dense grass in the meadow area, bare soil in the arable area and an extreme storm event; (b) vegetation cover everywhere and a lower intensity rainfall event. We compared the results of simulations with spatial distributions of observed colluvial deposits (Fig. 2(a)) and linear erosion features digitized from aerial photographs (Fig. 1(a)).

For case (a), prevailing *detachment limited* erosion is predicted for the bare soil area, due to the high transporting capacity of fast moving water. The net erosion $D(\mathbf{r}) \approx D_c(\mathbf{r})$ and almost all detached sediment is transported to the stream while deposition is restricted to small concave areas and channels (Fig. 1(b),(c)). This represents a situation close to the one observed after an extreme storm event in 1993 when extensive rilling occurred, with only 7% of eroded sediment deposited within the area (Auerswald *et al.*, 1996). For the second case with smaller transport capacities, the erosion process is close to *sediment transport capacity limited* case when $|\mathbf{q}_s(\mathbf{r})| \approx T(\mathbf{r})$, and the net erosion/deposition rate $D(\mathbf{r}) \approx \nabla\cdot[T(\mathbf{r})\mathbf{s}_0(\mathbf{r})]$, where $\mathbf{s}_0(\mathbf{r})$ is the unit vector in the steepest slope direction. The erosion rates are lower and the model predicts large extent of areas with deposition (Fig. 2(b),(c)). Such behaviour is close to the observed distribution of colluvial deposits (Fig. 2(a)). For this case, terrain shape plays an important role as demonstrated by a theoretical relationship (Mitas & Mitasova, 1998) for net erosion/deposition

$$D(\mathbf{r}) = K_f \rho_w g \{[\nabla h(\mathbf{r})]\cdot\mathbf{s}_0(\mathbf{r}) \sin\beta(\mathbf{r}) - h(\mathbf{r})[\kappa_p(\mathbf{r})+\kappa_t(\mathbf{r})]\}$$

where $\kappa_p(\mathbf{r})$ is the profile curvature, $\kappa_t(\mathbf{r})$ is the tangential curvature (for curvature definitions see Mitasova & Hofierka, 1993). From the point of view of land-use management, it is important to note that for both simulations (a), (b) the highest rates of net erosion as well as net deposition were predicted in hollows with high concentrated sediment flow (Figs 1(b),(c); 2(b),(c)). Field measurements confirm that

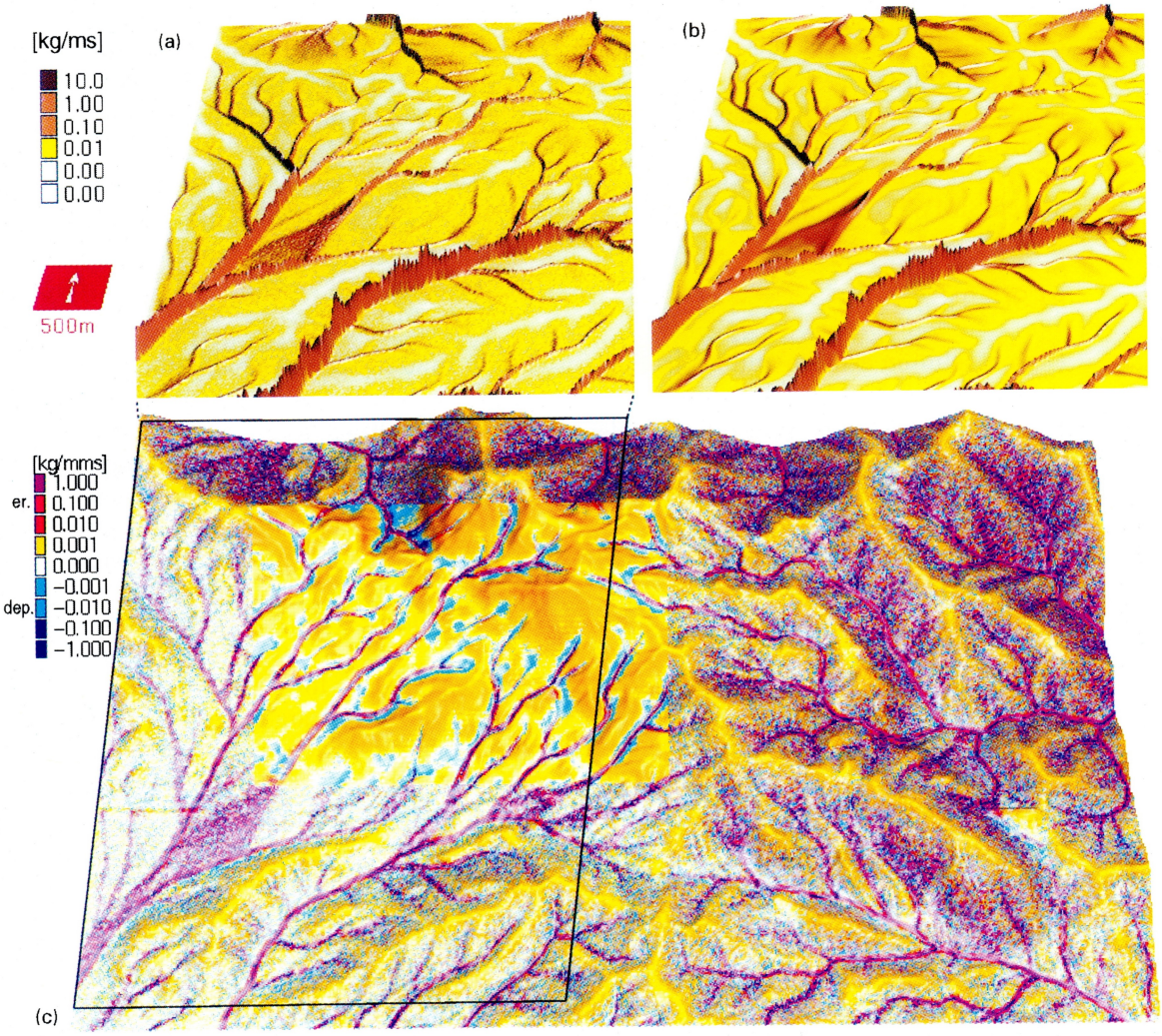

Fig. 4 Illustration of the Green's function Monte Carlo method and its multi-scale implementation: (a)sediment flow rates estimated with 20 000 sampling points and (b) 2 million sampling points; (c) net erosion/deposition estimated with spatially variable resolution and accuracy.

this area has the thickest layers of colluvial deposits but also large linear erosion features were observed here after a strong storm (Auerswald *et al.*, 1996). The second highest erosion is predicted on upper convex parts of hillslopes where the highest loss of radio-tracers and the lowest yields were observed (Auerswald, personal communication). Increased erosion is predicted also for bare narrow stripes below the grass areas, where water accelerates after depositing the sediment. The major difference in spatial patterns between the two modelled cases is the spatial extent of erosion/deposition. In the simulation (a) 93% of the area experienced

erosion while simulation (b) predicted erosion only for 70% of the area, with extent of deposition close to the observed spatial distributions of colluvial deposits. Deposition was also predicted at the upper edges of meadows, where the rills follow the borderline between the grass and bare soil areas and where deposits were found in the upper convex part of the grassy hillslope (Figs 1 and 2).

We have investigated the possibility of employing the simulations for improving erosion prevention using the following approach. For the traditional land use, ≈ 30% of the area was covered with grass. To find a more effective distribution of this protective grass cover, we used the presented model to identify areas with the highest erosion risk assuming uniform bare soil and then redistributed the same extent of grass cover to these high risk areas (Fig. 3(a)). The simulation of erosion/deposition for the new, computer generated land-use design demonstrates its potential to dramatically reduce erosion and sediment loads, especially in hollows (Fig. 3(b),(c)). It is interesting to note that the land-use design obtained by this rather simple computational procedure, based on elevation data, has several common features with the sustainable land-use design proposed and implemented in 1993 at the farm (Auerswald *et al.*, 1996).

Simulations with spatially variable resolution and accuracy for large areas

To illustrate the capability of the presented approach to simulate erosion/deposition patterns at spatially variable accuracy/resolution we have applied the model to a 36 km^2 mountainous area at 20-m resolution, with more detailed predictions (10-m resolution) within a potential high intensity use 7 km^2 subarea targeted for rehabilitation. Detailed solution for the entire area would require about 2 million samples applied to 360 000 grid cells. With spatially variable resolution significant savings in processing time can be achieved by using only 20 000 samples for 75 000 cells covering the entire study area at 20-m resolution, and a higher density sampling (2 million) used only for the targeted area represented by 50 000 cells (10-m resolution). The predicted sediment flow and erosion/deposition patterns have a detectable level of noise in low resolution areas, while the distributions in the targeted subarea are modelled with a high level of detail (Fig. 4). Further investigation will be performed into the error propagation from low to high resolution areas and its dependence on the location of subarea within the basin structure.

Acknowledgements We would like to thank K. Auerswald from the Technical University Munich, Germany, and S. Warren from the USA Construction Engineering Res. Labs for providing the field data and for valuable discussions. We acknowledge the support by the Strategic Environmental Research and Development Program.

REFERENCES

Auerswald, K., Eicher, A., Filser, J., Kammerer, A., Kainz, M., Rackwitz, R., Schulein, J., Wommer, H., Weigland, S. & Weinfurtner, K. (1996) The Scheyern project of the FAM. In: *Development and Implementation of Soil Conservation Strategies for Sustainable Land Use* (ed. by H. Stanjek) (Int. Congress of ESSC, Tour Guide II), 25–

68. Technische Universitaet Muenchen, Freising-Weihenstephan, Germany.

Flanagan, D. C. & Nearing, M. A. (eds) (1995) *Water Erosion Prediction Project*. Report no. 10, National Soil Erosion Laboratory, USDA ARS, West Lafayette, Indiana, USA.

Foster, G. R. & Meyer, L. D. (1972) A closed-form erosion equation for upland areas. In: *Sedimentation: Symposium to Honor Prof. H. A. Einstein* (ed. by H. W. Shen), 12.1–12.19. Colorado State University, Fort Collins, USA.

Gardiner, C. W. (1985) *Handbook of Stochastic Methods for Physics, Chemistry, and the Natural Sciences*. Springer, Berlin.

Maidment, D. R. (1996) Environmental modeling within GIS. In: *GIS and Environmental Modeling: Progress and Research Issues* (ed. by M. F Goodchild, L. T. Steyaert & B. O. Parks), 315–324. GIS World, Fort Collins, USA.

Mitas, L. (1996) Electronic structure by Quantum Monte Carlo: atoms, molecules and solids. *Computer Physics Communications* **97**, 107–117.

Mitas L. & Mitasova, H. (1998) Distributed soil erosion simulations for effective landuse management. Accepted for *Wat. Resour. Res.* **34**(3), 505–516.

Mitas, L., Brown, W. M. & Mitasova, H. (1997) Role of dynamic cartography in simulations of landscape processes based on multi-variate fields. Computers & Geosci. **23**, 437–446.

Mitasova, H. & Mitas, L. (1993) Interpolation by regularized spline with tension:

I. Theory and implementation. Math. Geol. **25**, 641–655.

Mitasova, H. & Hofierka, J. (1993) Interpolation by regularized spline with tension: II. Application to terrain modeling and surface geometry analysis. Math. Geol. **25**, 657–669.

Mitasova, H., Mitas, L., Brown, W. M., Gerdes, D. P., Kosinovsky, I. & Baker, T. (1995) Modelling spatially and temporally distributed phenomena: new methods and tools for GRASS GIS. Int. J. Geogr. Inform. Systems **9**, 433–446.

Moore, I. D., Turner, A. K., Wilson, J. P., Jensen, S. K. & Band, L. E. (1993) GIS and land surface–subsurface process modeling. In: *Geographic Information Systems and Environmental Modeling* (ed. by M. F Goodchild, L. T. Steyaert & B. O. Parks), 196–230. Oxford University Press, New York.

Nearing M. A., Norton, L. D., Bulgakov, D. A., Larionov, G. A., West, L. T. & Dontsova, K. M. (1997) Hydraulics and erosion in eroding rills. Wat. Resour. Res. **33**, 865–876.

Saghafian, B., Julien, P. Y. & Ogden, F. L. (1995) Similarity in catchment response: 1. Stationary rainstorms. Wat. Resour. Res. **31**(6), 1533–1541.

Suri, M. & Hofierka, J. (1994) Soil water erosion identification using satellite and DTM data. In: *Proceedings of the EGIS/MARI '94 Conference* (Paris, France), 937–944.